

1 **E156G and Arg158, Phe-157/del mutation in NTD of spike protein in B.1.617.2 lineage of**
2 **SARS-CoV-2 leads to immune evasion through antibody escape**

3 **Armi M Chaudhari¹, Dinesh Kumar¹, Madhvi Joshi¹, Amrutlal Patel¹, and Chaitanya**
4 **Joshi^{1*}**

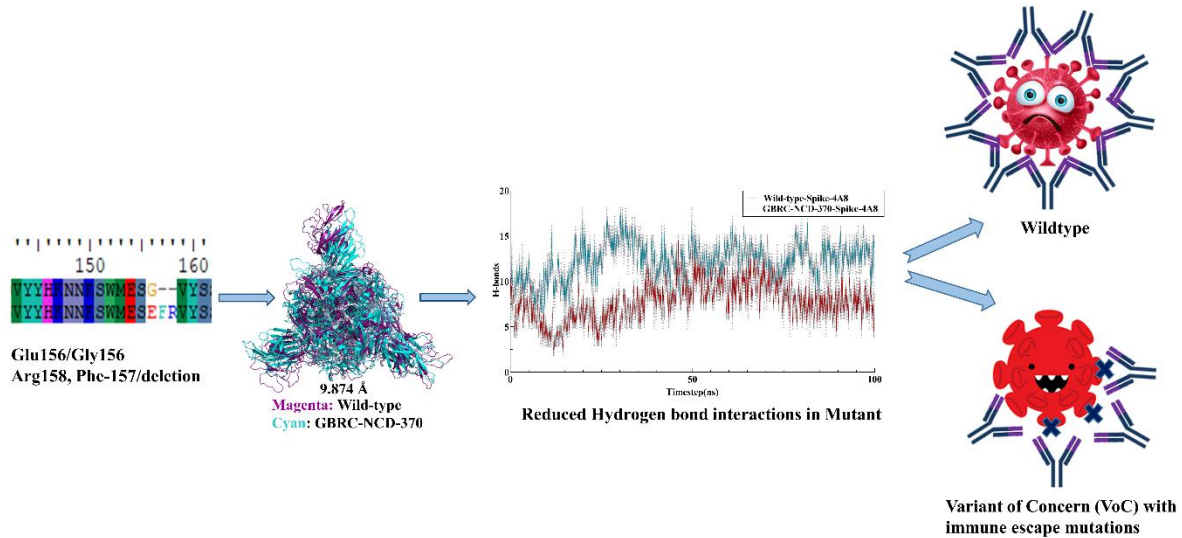
5 ¹Gujarat Biotechnology Research Centre (GBRC), Department of Science and Technology,
6 Government of Gujarat, Gandhinagar-382011

7 ***Corresponding author:** Chaitanya Joshi, Gujarat Biotechnology Research Centre (GBRC),
8 Department of Science and Technology, Government of Gujarat, 6th Floor, Block B&D, MS
9 Building, Gandhinagar-382011. **Tel/Fax:** 079-232-58680; **E-mail:** director@gbrc.res.in

10 **Abstract**

11 Emerging variants of SARS-CoV-2 with better immune escape mechanisms and higher
12 transmissibility remains a persistent threat across the globe. B.1.617.2 (Delta) variant was
13 first emerged from Maharashtra, India in December, 2020. This variant is classified to be a
14 major cause and concern of the second wave of COVID-19 in India. In the present study, we
15 explored the genomic and structural basis of this variant through computational analysis,
16 protein modelling and molecular dynamics (MD) simulations approach. B.1.617.2 variant
17 carried E156G and Arg158, Phe-157/del mutations in NTD of spike protein. These mutations
18 in N-terminal domain (NTD) of spike protein of B.1.617.2 variant revealed more rigidity and
19 reduced flexibility compared to spike protein of Wuhan isolate. Further, docking and MD
20 simulation study with 4A8 monoclonal antibody which was reported to bind NTD of spike
21 protein suggested reduced binding of B.1.617.2 spike protein compared to that of spike
22 protein of Wuhan isolate. The results of the present study demonstrate the possible case of
23 immune escape and thereby fitness advantage of the new variant and further warrants
24 demonstration through experimental evidence. Our study identified the probable mechanism
25 through which B.1.617.2 variant is more pathogenically evolved with higher transmissibility
26 as compared to the wild-type.

27 **Keywords:** SARS-CoV-2, COVID-19, Spike protein, Antibody, MD simulations and
28 Docking



29

30 1. Introduction

31 India is witnessing the peak of another COVID-19 wave with over 0.32 million casualties
32 since 2020, and more than 27.4 million confirmed positive cases as per WHO reports
33 accessed on 27th May, 2021. Genome surveillance is a powerful tool to study the viral
34 genomic profile, variants of concern and their epidemiological significance in disease
35 outbreak outcome of the patients. All coronaviruses are positive-sense RNA viruses
36 belonging to the order *Nidovirales* and family *Coronaviridae*. They are characterized by
37 crown-like spikes on their surfaces and large enveloped genome of ~30 kilobases size. The
38 SARS-CoV-2 genome contains four major structural proteins: spike (S), membrane (M),
39 envelope (E), and nucleocapsid (N) protein. The spike (S) protein mediates entry and
40 attachment of the coronavirus to the host cell surface receptors resulting in fusion and viral
41 entry in the hosts. The membrane (M) protein defines the shape of the viral envelope while
42 the envelope (E) protein and nucleocapsid (N) protein participates in viral assembly and
43 budding of the virion complex in the infected cells [1,2]. SARS-CoV-2 uses ACE2 receptor
44 for host cell entry and the spike protein of SARS-CoV-2 is primed by TMPRSS2 while the
45 role of several other host receptors is partially explored with limited information that may
46 determine the altered virulence and pathogenicity of the evolving SARS-CoV-2 lineages
47 around the globe. SARS-CoV-2 possesses highly efficient and evolved strategies for
48 proteolytic activation of spike, and host proteases have been shown to proteolytically process
49 the spike protein. These include, but are not limited to, endosomal cathepsins, cell surface
50 trans-membrane protease/serine (TMPRSS) proteases, furin, and trypsin that are critical
51 determinants of the virus entry and pathogenesis in humans [3,4]. SARS-CoV-2, in
52 comparison to SARS-CoV, contains a polybasic sequence motif, Arg-Arg-Ala-Arg (RRAR),
53 at the S1/S2 boundary, furin-type cleavage site in its spike protein, which when cleaved can
54 bind and activate neuropilin receptors. Further, research studies indicate that NRP1 enhances
55 SARS-CoV-2 infectivity and is highly expressed in respiratory and olfactory epithelium [5].

56 Under the prevailing circumstances, the immune response of the patients plays a significant
57 role in determining the disease fighting ability of the body. A myriad of various cell types
58 such as macrophages, alveolar epithelial cells, lymphoid cells, and dendritic cells (DCs) have
59 a major role in the first line of defense. Once the immune system is triggered for the entry of
60 foreign viral pathogens inside the body and that breached the first lines of defense system,
61 several specific molecular and inter-cellular signaling cascades ensure the establishment of
62 the body's immune response [6,7]. When the invading respiratory viruses evolve mechanism
63 that either circumvent or suppress the innate immune responses to create a window of
64 opportunity for efficient virus replication, thereby often causing disease. The affected innate
65 immune response also impacts subsequent adaptive immune responses, and therefore viral
66 innate immune evasion often undermines fully protective immunity such as lack of virus
67 neutralizing antibodies [8–11]. Further, genetic makeup and evolution in virus also enable
68 them to develop mutations that can cause immune escape and immune evasion in the hosts,
69 thereby increasing the chances of severity and virulence of the pathogenic variants [12].
70 These variants, which are observed with features such as higher transmissibility are
71 categorized as Variants of Concern (VoC) by Public Health England (PHE), UK; CDC, USA,
72 and World Health Organization (WHO) based on their risk assessment criteria of infection
73 severity, susceptibility geographical prevalence, and transmission in humans. Therefore,
74 genomic surveillance studies are essential in monitoring these variants that may even arise in
75 the future pandemics.

76 New variants of SARS-CoV-2 are emerging challenge for scientific community and public
77 health system in the different geographical regions across the globe. These variants, have
78 been designated as Variant of Concern (VoCs) which has noticeable higher transmissibility
79 and probably more virulent compared to other variants. Genomic structure of such variants
80 suggests that they were evolved to escape the immune system of the host thereby giving them
81 the fitness advantage and thus increased spread among the population. Further, research is
82 needed to establish the mechanism of escape and potential host genetic factor that might help
83 in these evolved pathogenic viral strains of SARS-CoV-2.

84 Furthermore, understanding of the role of virus-host interactions and immune response during
85 these SARS-CoV-2 infections will be pivotal to ultimately meet these evolving challenges.
86 Eventually, efficacy of the combined innate and adaptive responses is on the host's side,
87 while the virulence and its capacity to evade the host's immune responses is on the virus' side,
88 together, the balance between them dictate the disease outcome in the context of the host-
89 virus interactions. Recent studies on spike protein interactions with monoclonal antibodies
90 4A8 suggests that N- terminal domain is essential binding site for 4A8 [13]. Some prominent
91 mutations (>99.7% frequency) in virus favors the virus like D614G [14] and some favors the
92 host like C241T [15]. To find the same, this research focus on the mutations in N-terminal
93 domain in B.1.617.2 (now delta) lineage of SARS-CoV-2 and its impact on protein structural
94 changes and antibodies binding using molecular modeling and dynamics approach.

95 **2. MATERIAL AND METHODS**

96 **2.1 Protein complexes used for this study**

97 Variants of Spike protein from SARS-CoV-2 were taken into study. Mutated spike from
98 SARS-CoV-2 used in this study were derived from amino acid sequence submitted in
99 GAISAD with accession number EPI_ISL_2001211. Reference protein with PDB id 7KRQ
100 was used for homology modelling.

101 **2.2 Protein modelling and Molecular dynamics simulations**

102 Homology modelling panel implemented in Schrodinger suite release 2021-1 was used to
103 build mutated spike protein with reference protein 7KRQ. Sequence was imported and
104 homology blast search was performed. Crystal structure of 7KRQ was imported in to maestro
105 and protein complex refinement was performed using protein preparation wizard [16].
106 Missing side chains were added through PRIME and pKa refinement was done with epik
107 [17]. Molecular dynamics simulation for spike protein and Spike-antibody complexes were
108 performed in Schrodinger suite 2021-1 implemented DESMOND till 100 nanoseconds (ns)
109 [18]. Protein structures were refined using OPLS4 force field and altered hydrogen bonds
110 were refilled using structure refinement panel implemented in Schrodinger[19][20]. Particle
111 mesh Ewald method is applied to calculate long range electrostatic interactions. [21]. The
112 trajectories were recorded at every 1.2 ps intervals for the analysis. TIP3P water molecules
113 were added and 1.5 M Salt concentration was added to neutralize the system [22]. The
114 Martyna–Tuckerman–Klein chain coupling scheme with a coupling constant of 2.0 ps was
115 used for the pressure control and the Nosé–Hoover chain coupling scheme for temperature
116 control [23]. MD simulations were performed at 310.3K temperature. The behaviour and
117 interactions between the protein and protein were analyzed using the Simulation Interaction
118 Diagram tool implemented in Desmond MD package. The stability of complex was
119 monitored by examining the RMSD of the protein and protein atom positions in time.
120 PYMOL was used for obtaining high resolution images [24]. Protein modelling and
121 Molecular dynamics simulations were performed into duplicates.

122 **2.3 Molecular docking of Spike protein with monoclonal antibodies using spike and** 123 **affinity prediction**

124 Variants of spike proteins Wildtype (7KRQ) and Mutant (GBRC-NDC-370) were docked
125 with monoclonal antibody 4A8. Protein structures were prepared using protein-preparation
126 wizard [16]. After structure refinement of protein, PIPER was used for the protein-protein
127 docking [25]. For binding residues (as shown in figure 2A) detection among both receptor
128 (spike) and ligand (antibody-4A8) attraction forces were applied with $<3\text{\AA}$ cut off. 70000
129 docking poses were checked for fulfilling the criteria of distance restrains applied for the
130 binding sites residues. Recently deposited crystal structure of spike protein binding with
131 monoclonal antibody was taken for applying the restraint file showing list of spike residues
132 binding with residues of 4A8. Top 30 poses were generated and a pose with highest free glide
133 energy was used for the MD analysis.

134 Alanine residue scanning was performed for the binding affinity prediction in PDB deposited
135 spike antibody complex with id 7C2L [13]. Binding site residues were mutated to alanine in
136 order to bind the pivotal residues involved into direct binding with antibody. Positive value of
137 Δ affinity indicated that while mutating binding sites residues to alanine, binding is hindered

138 due to small side chains of alanine and which in terms implies that those important residues
139 were essential for direct affinity with antibody [26,27]. Residue alanine scanning panel
140 present in Biologics of Schrodinger 2021-1 is used to perform the above task.

141 **2.4 Binding energy calculation**

142 Binding energy for protein-protein complex was calculated in the form of Prime Molecular
143 Mechanics-Generalized Born Surface Area (MMGBSA) using thermal_mmgbsa.py
144 implemented in PRIME module of Schrodinger [28–30]. ΔG of protein-protein complex was
145 calculated using following equation.

$$146 \quad \Delta G_{\text{Bind}} = \Delta G_{\text{SA}} + \Delta G_{\text{Solv}} + \Delta E_{\text{MM}}$$

147 VSEB solvation model and OPLS4 force-field were used for calculation of MMGBSA.
148 Protein-protein complex system seems to have stable RMSD pattern after 60ns. These frames
149 were used to calculate MMGBSA. First energy minimized structure out of 30 was used to
150 find dominant interacting residues among spike. Interaction image was taken in new version
151 of Schrodinger 2021-2 where protein-protein interaction images can be taken in Biologics.

152 **2.5 Dynamics cross-correlation matrix (DCCM) and Principal Component analysis (PCA)**

154 Correlative and anti-correlative motions play a vital role in recognition and binding in a
155 biological-complex system which can be prevailed by MD simulation trajectory by
156 determining the covariance matrix about atomic fluctuations [31]. The extent of correlative
157 motion of two residues (or two atoms or proteins) can be symbolized by the cross-correlation
158 coefficient, C_{ij} . It is defined by following equation:

$$159 \quad C_{ij} = \frac{\langle \Delta r_i \cdot \Delta r_j \rangle}{(\langle \Delta r_i^2 \rangle \langle \Delta r_j^2 \rangle)^{1/2}} \quad \dots \text{eq: 1}$$

160 From above equation, i (j) explains i^{th} (j^{th}) two residues (or two atoms or proteins), Δr_i (Δr_j)
161 is the displacement vector corresponding to i^{th} (j^{th}) two residues (or two atoms or proteins),
162 and $\langle \dots \rangle$ stand for the ensemble average. The value of C_{ij} is from 1 to -1. $+C_{ij}$ implies
163 positively correlated movement (the same direction) indicated into blue color, and $-C_{ij}$
164 implies anti-correlated movement (opposite direction) indicated into red color. The higher the
165 absolute value of C_{ij} is, the more correlated (or anti-correlated) the two residues (or two
166 atoms or proteins).

167 PCA is an implicit tool to unsheathe the essential information from MD trajectories by
168 pulling out global slow motions from local fast motions[32]. To perform PCA, the covariance
169 matrix C was calculated initially. The elements C_{ij} in the matrix C are defined as:

$$170 \quad C_{ij} = \langle (r_i - \langle r_i \rangle) * (r_j - \langle r_j \rangle) \rangle \quad \dots \text{eq: 2}$$

171 From equation 2, r_i and r_j are the instant coordinates of the i^{th} or j^{th} atom, $\langle r_i \rangle$ and $\langle r_j \rangle$ and
172 mean the average coordinate of the i^{th} or j^{th} atom over the ensemble. The principal
173 components (PCs) were calculated by diagonalization and obtaining the eigenvectors and
174 eigenvalues for the covariance matrix C . The principal components (PCs) are the projections

175 of a trajectory on the principal modes, of which usually the first few ones are largely
176 responsible for the most important motions. DCCM and PCA both were analyzed using
177 Schrodinger 2021-1 implemented python script *run trj_essential_dynamics.py* script of
178 Desmond [18].

179 **3. Result and discussion**

180 Spike protein of SARS-CoV-2 is known to bind ACE-2 receptor mediating virus entry. Spike
181 protein is more prone to mutations. For better penetrance viral spike had gone through several
182 mutations like D614G for increasing spike density and infectivity, E484K for reducing the
183 antibody neutralization, N501Y and K417N for altering spike interacting with human ACE
184 and human derived antibody [33–35]. Our study focuses on major deletion occurred in NTD
185 of spike protein at nucleotide position 22029-22035 (6bp) which in-terms induce 2 amino-
186 acid deletions Arg158, Phe-157/del and one amino acid mutation E156G.

187 **3.1 Mutational landscape of spike protein and its effects with respect to B.1.617.2 lineage**

188 Mutations listed in table 1, were impacting major structural change or not were studied
189 through structural alignment of both variants of spike proteins in Pymol. Superimposed
190 structure of wild-type and GBRC-NCD-370 spike with alignment RMSD 6.905 Å was shown
191 in figure 1A. RMSD value higher than 1Å suggests that these mutations were imparting
192 significant structural change in both variants of spike [36]. Among the list of overall
193 mutations, unique mutations Arg158, Phe-157/del and E156G were falling in NTD of spike.
194 Figure 1D, explains the effect of these mutations in changing amino acids conformation in
195 ball and stick form. One can visualize the difference in alignment of amino acids in NTD
196 within both variants which in terms effects the change in intermolecular contacts within spike
197 (Figure 1E). GBRC-NCD-370 showed intermolecular 5 hydrogen bonds and 6 hydrophobic
198 and aromatic contacts, which is way to higher than 2 hydrogen bonds and 1 hydrophobic
199 interaction seen in wild type spike. These intermolecular interactions are further enhancing
200 the rigidity and reducing the flexibility within NTD of GBRC-NCD-370. To correlate these
201 findings with MD simulations RMSD and RMSF were analyzed to further comment on
202 flexibility of GBRC-NCD-370.

203 RMSD (Root mean square deviation) for wild-type and GBRC-NCD-370 complex observed
204 were 5.89 ± 0.026 and 2.54 ± 0.018 , respectively (figure1G). RMSD graph is clearly narrating
205 that mutations in GBRC-NCD-spike protein are enhancing its stability compared to the wild-
206 type trimeric complex (figure1H). RMSF (Root mean square fluctuation) was 3.6 fold lower
207 in NTD of GBRC-NCD-370 spike compared to the wild-type complex. Decreased RMSF in
208 NTD explains reduced flexibility of amino acid residues within the region. Aurélie Bornot et
209 al 2010 precisely explains the protein flexibility in terms of RMSF and B-factors, where
210 increasing in RMSF values is related to increased change in protein conformation. In some
211 cases, amino acid residues are flexible though RMSF can be rigid through B-factors [37]. In
212 our case, protein seems to be flexible in both cases through RMSF and B-factors
213 (Supplementary figure S2). While no major change was observed with respect to other part of
214 protein. As NTD is binding site of wide variety of monoclonal antibodies, rigidization in that
215 region further affects the binding of antibody within both variants of spike. Principle

216 component analysis was performed where first dominant dynamic mode PC1 among the
217 trajectories were analyzed in VMD. Porcupines plots showing the projection of mode vectors
218 based on the residue fluctuation throughout the trajectories were shown in Figure 2C. Length
219 of mode-vectors in wild-type complex was higher compared to GBRC-NCD-370, which
220 suggests that overall NTD flexibility is decreased in B.1.617.2 lineage. Increase in
221 intermolecular contacts in mutated region further support the rigidization of GBRC-NCD-370
222 (figure1E).

223 Mutations in NTD were covering the binding domain for monoclonal antibodies (Figure 2A).
224 PDB id 7CL2 was chosen as a wild-type complex of spike with 4A8 monoclonal antibody.
225 GBRC-NCD-370 variant was docked with 4A8 was chosen as mutant complex. Glide energy
226 of wild type A48 and GBRC-NCD-4A8 were -115.64 and -68.74 respectively. More
227 negative energy score was showing enhance binding among protein-protein complex.
228 MEDUSA five class predictions narrate the decrease in flexibility by 2% for the GBRC-
229 NCD-370 compared to wild-type (Figure 2B & 2C). Spike flexibility and rigidity were
230 analyzed in term of its binding with monoclonal antibodies by performing alanine residue
231 scanning (Figure 2D). Wild-type-4A8 was processed through residue scanning with alanine
232 mutagenesis to investigate the important residue for the binding with 4A8. Amino acid
233 residues Y145, K147, 150K, 152W, 156E, 157F, and 158R showed positive binding affinity
234 values with 4A8 upon mutating these residues to alanine (Figure 2D). These results clearly
235 indicate that the mutations in the NTD domain of spike caused decrease in binding of 4A8
236 antibody in B.1.617.2 lineage. To further explore the effect, the mutations in NTD with
237 respect to affinity with 4A8, MD simulations were performed in duplicates and binding
238 energies among both variants were analyzed.

239 **3.2 Effect of Arg158, Phe-157/del and E156G in N- terminal domain with respect to the** 240 **host immunity**

241 MD simulations of both mutant and wild type spikes with 4A8 antibody explored the effect
242 of mutation Arg158, Phe-157/del and one amino acid mutation E156/G in terms binding with
243 monoclonal antibodies and depict the case of immune evasion. RMSD of GBRC-NCD-370-
244 4A8 and wildtype-4A8 was $20.147 \pm 0.526 \text{ \AA}$ and $16.142 \pm 0.453 \text{ \AA}$, respectively (Figure 3A). In
245 GBRC-NCD-370-4A8 platue was reached after 65 ns and jumps were observed during the
246 MD simulations, while wildtype-4A8 was found to be stable after 20ns only. These major
247 difference among the both trajectories shows that GBRC-NCD-370-4A8 complex is 4 fold
248 less stable than wildtype-4A8. Hydrogen bonds formation within GBRC-NCD-370-4A8
249 complex was 6 fold lower compared to wildtype-4A8 (figure 3B). Decrease in hydrogen bond
250 formation clearly indicates reduced interaction of antibodies in B.1.617.2 lineage.

251 Binding energy among the complex was analyzed through MMGBSA. Major energies
252 contributing to the complex formation were elucidated in table 2 with bold text. Spike-4A8
253 complex formation is driving through the major electrostatic, covalent, ionic-interactions,
254 lipophilic (hydrophobic) and Vander-Waals interactions within both complexes. Overall free
255 energy binding ΔG in wild-type and GBRC-NCD-370 complex is -119.086 ± 19.42 and $-$
256 55.496 ± 14.57 , respectively. Interaction in energy minimized structure obtained through
257 MMGBSA approach is shown in figure 3E & 3F. In wild-type complex overlapping strong

258 interaction between charged negative (orange) and charge positive residues (blue) is way
259 higher compare to mutant. For example A-Lys147: B-Glu72, A-Lys150: B-Glu57 & B-Glu55
260 were forming hydrogen bonds and salt bridges in spike (A) and 4A8 (B). Jason E Donald and
261 group suggests that salt bridges were geometric specific and designable interactions [38,39].
262 Lys150 is forming salt bridge and hydrogen bonds with two negative charged amino acids
263 Glu57 and Glu55 (Figure 3E & 3F). These kind of favorable interactions are formed in wild-
264 type spike but absent in GBRC-NDC-370, leads to conclude that geometry of NTD in spike
265 had changed as such that it is reducing the strong interaction with 4A8 in GBRC-NCD-370
266 (mutant) (Table:2). This kind of salt-bridges are favorable exist in hydrophobic environment
267 [40], leads to higher lipophilic energy in wild type (-30.334 Kcal/mole) compare to GBRC-
268 NCD-370 (-11.9757Kcal.mole). Overall Wildtype spike seems to have better binding with
269 monoclonal antibodies compared to the GBRC-NCD-370, which leads to conclude that there
270 is possible case of immune evasion among B.1.617.2 lineage.

271 Dynamics cross-correlation matrix (DCCM) of wild-type and GBRC-NCD-370 spikes with
272 4A8 is shown in figure 3. In DCCM wild-type-spike-4A8 is showing higher intensity of blue
273 color compared to the GBRC-NCD-370-spike-4A8. Positive C_{ij} values indicate blue colors
274 leads to better interaction profile between those residues. NTD region covers 17-305 amino
275 acid residues where major residue contributing in direct contact was shown in figure 2. In the
276 region covering orange arrow (antibody 4A8) intensity of blue color is higher, indicating
277 more positive cross correlation with respect to NTD region of spike wild-type compare to
278 GBRC-NCD-370. In wild-type complex NTD residues have showing higher negative cross-
279 correlation compare to GBRC-NCD-370 (Figure 3C &3D). Results of negative cross-
280 correlations in some regions were completely correlating with change in flexibility of NTD.
281 Higher intensified positive cross-correlation showed structural compactness among the NTD
282 in GBRC-NCD-370, which can be unfavorable for the antibody binding. Overall cross-
283 correlation among 4A8 which were shown in box a and b with respect to spike, were positive
284 in wild-type and negative in GBRC-NCD-370 supporting the case of antibody escape.

285 **4. Conclusion**

286 The present study addressed the critical structural and genomic determinants of the SARS-
287 CoV-2 (B.1.617.2/Delta) variant which is most dominant in India during the second wave and
288 spreading quickly in different geographical regions of the globe. The E156G and Arg158,
289 Phe-157/del mutations in NTD of spike protein of SARS-CoV-2 (B.1.617.2/Delta) variant
290 showed more rigidity and reduced flexibility compared to Wuhan isolate. Further, our study
291 showed possible case of immune escape by demonstrating reduce binding of mutant spike
292 compared to Wuhan isolate with reported antibody known to bind NTD of spike protein
293 thereby providing insights into the structural basis and highlight the impact of the key
294 mutations for the higher transmissibility, pathogenicity and virulence. Therefore, it is
295 important to better monitor and identify the new emerging variants of SARS-CoV-2 using
296 genome sequencing and surveillance that may have increased transmission, virulence and
297 altered antigenicity evolved over time for epidemiological significance.

298 **Credit authorship and contribution statement**

299 AC performed all Insilco experiments, analysis, writing original draft preparation, data
300 curation. DK analyzed the sequences, write and edited the manuscript. AP, MJ, CJ writing
301 review and editing, supervision, project administration, funding acquisition

302 **Acknowledgement**

303 Authors would like to acknowledge Department of Science and Technology (DST),
304 Government of Gujarat for infrastructure support for the research work. We also thank
305 Gujarat University for providing us GPU accelerated computer facility to enhance the speed
306 of our work.

307 **Funding**

308 Funding was provided by Department of Science and Technology (DST), Government of
309 Gujarat, Gandhinagar, India.

310 **Declaration of Competing Interest**

311 The authors declare that they have no known competing financial interests or personal
312 relationships that could have appeared to influence the work reported in this paper.

313

314

315

316

317

318

319

320

321

322

323

324

325 **Tables and Figures**

326 **Table 1:** List of spike protein mutation present in GBRC-NCD-370

Sr. No	Amino Acid Change
1	T19R
2	G142/D
3	del157/158/ R156G

4	R452G
5	A222V
6	L452R
7	T478K
8	D614G
9	P681R
10	D950N

327

328 **Table 2:** Differences in energy components contributing to Complex formation within Wild-
329 type (7KRQ) and Mutated GBRC-NCD-370 monoclonal antibodies (4A8).

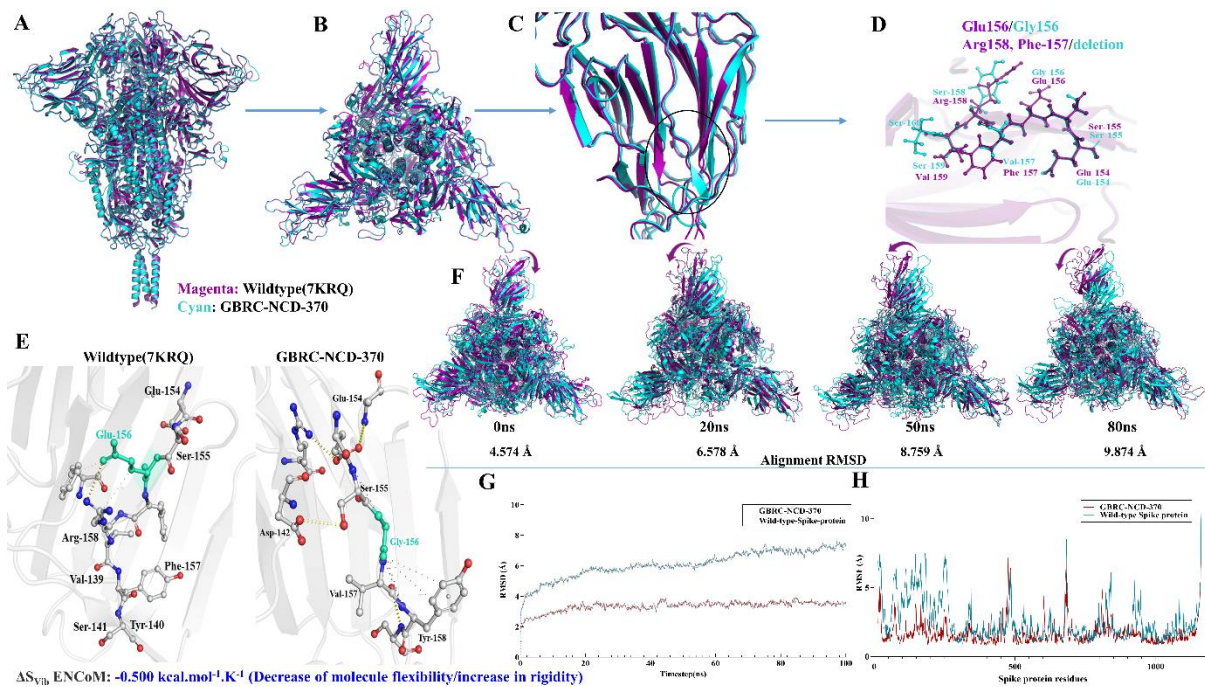
Energy components	Wildtype-4A8	GBRC-NCD-370-4A8
Glide energy	-115.64	-68.74
ΔG Binding	-119.0869622	-55.4968
ΔG Electrostatic energy	-791.09011	-357.715
ΔG Covalent energy	-14.19260182	-7.50638
ΔG Hbonds energy	-8.385258773	-5.17996
ΔG Lipophilic energy	-30.33398583	-11.9757
ΔG pi piinteraction energy	-2.106536604	1.156437
ΔG selfcontactcorrelation	-0.023560517	-0.15669
ΔG Solv_GB	781.5183498	434.7153
ΔG vdw energy	-82.85846217	-108.834

330

331

332

333 **Figures**



334

$\Delta S_{vib, ENCoM}$: -0.500 kcal.mol⁻¹.K⁻¹ (Decrease of molecule flexibility/increase in rigidity)

335 **Figure 1: Rigidity and reduce in flexibility of N-Terminal domain of spike protein.**

336 **1A:** 3D Structural alignment of wild-type [7KQR] and GBRC-NCD-370 trimetric spike

337 proteins with superimposition RMSD value: 6.356. Wild-type protein is shown in magenta

338 and GBRC-NCD-370 is shown in cyan color. **1B:** Top view of trimetric spike protein. **1C &**

339 **1D:** Focusing structural difference in NTD of wild-type and GBRC-NCD-370 spike protein.

340 **1E:** Intermolecular contacts between wild-type and mutant spike protein. **1F:** Frame

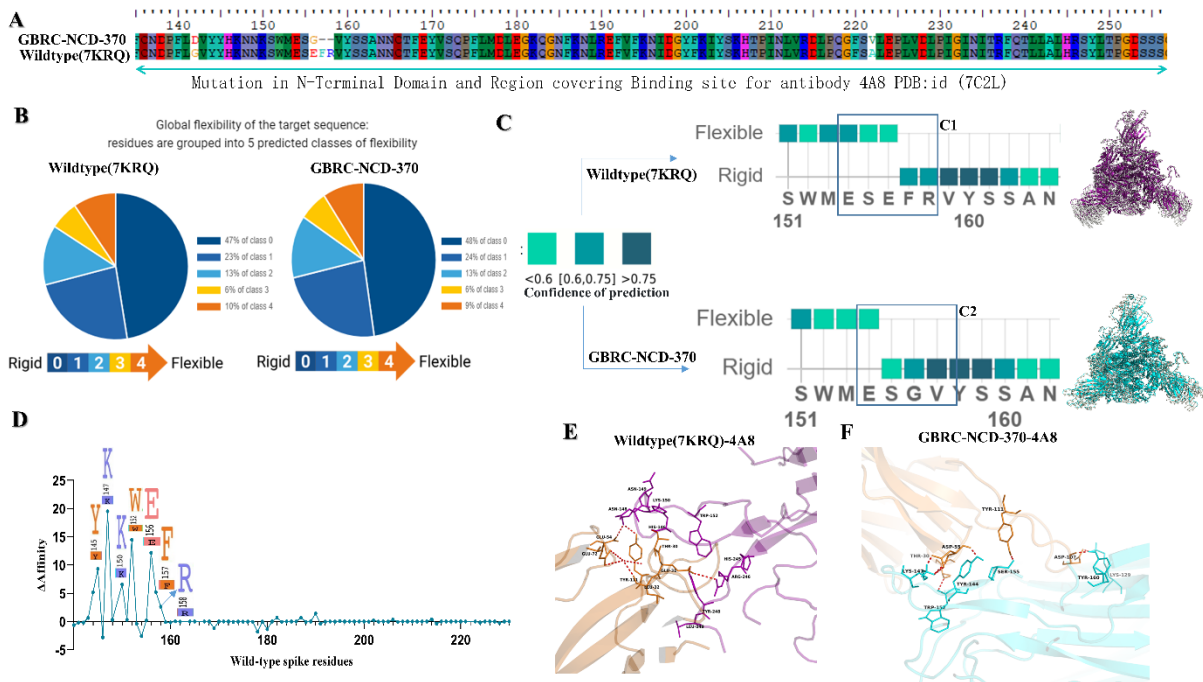
341 superimposition of wild-type and GBRC-NCD-370 spike proteins for visualization of

342 dynamics modes depicting difference in NTD. Magenta colored arrow showing dynamic

343 moments of wild-type spike. **1G & 1H:** RMSD and RMSF plot generated from MD-

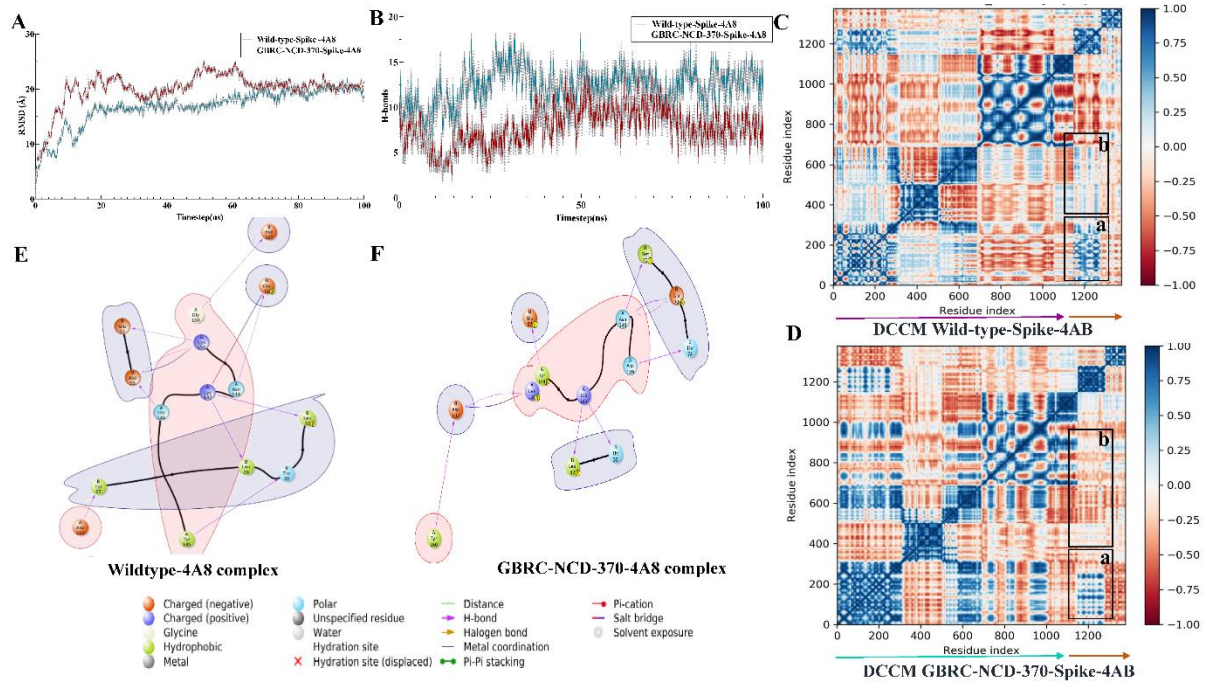
344 Simulation respectively. Wild-type protein is shown in deep teal color and GBRC-NCD-370

345 is shown in red color.



346

347 **Figure 2: Reduce flexibility influence the binding of monoclonal antibodies (4A8) with**
 348 **spike protein. 2A:** Amino acid residues falling in the binding region NTD of spike.
 349 Wildtype and mutated sequences were annotated with NCBI reference/accession id number
 350 MN986947.3 and GBRC-NCD-370 respectively. **2B:** Output generated from MEDUSA to
 351 determine change rigidity and flexibility among both variants. 5 predicted classes were
 352 generated in range of 0-4, where blue region explains rigid regions and yellow to orange
 353 regions explains the flexible regions among proteins. **2C:** Flexible and rigid regions in region
 354 covering mutation. Cyan to deep teal color represents the flexible to rigid region with COP
 355 (confidence of prediction) with <math>< 0.6</math> and >0.75 respectively. Porcupines plots generated from
 356 PCA analysis were also supporting the same were shown red tube conformation with mode
 357 vectors. **2D:** Alanine residues scanning of wildtype-4A8 complex. Residues important in bind
 358 with monoclonal antibodies were shown in logo plot with positive binding affinity. **2E:**
 359 Binding pose of Wildtype-4A8 complex. Spike is shown in magenta color while 4A8 is
 360 shown in orange color. Residues involved in pivotal contacts like hydrogen bonds (red) were
 361 shown in ball and stick conformation with black colored labels. **2F:** Binding pose of GBRC-
 362 NCD-370-4A8 complex. Spike is shown in cyan color while 4A8 is shown in orange color.
 363 Residues involved in pivotal contacts like hydrogen bonds (red) were shown in ball and stick
 364 conformation with black colored labels.



365

366

367 **Figure 3:** MD analysis of Spike-antibodies complexes. **3A:** RMSD (root mean square
 368 deviation) within Wildtype-4A8 (cyan) and gbrc-ncd-370-4A8 (mutant) complex. **3B:**
 369 Hydrogen bonds formation within Wildtype-4A8 (cyan) and gbrc-ncd-370-4A8 (mutant)
 370 complex. **3C:** Dynamics cross-correlation matrix obtained from trajectories analysis of wild-
 371 type-4A8 complex. Spike protein shown in magenta arrow and orange arrow is indicating
 372 4A8. **3D:** Dynamics cross-correlation matrix obtained from trajectories analysis of GBRC-
 373 NCD-370-4A8 complex. Spike protein shown in cyan arrow and orange arrow is indicating
 374 4A8. Blue to red color represents the c_{ij} values between 1 to -1. No cross correlation was
 375 shown by white color. **3E & 3F:** Energy minimized structure obtained through MMGBSA
 376 for Wildtype-4A8 and GBRC-NCD-370-4A8 respectively. Positive charged, negative
 377 charged amino acid residues were shown in orange and blue color respectively

378 References

379 1. Gordon DE, Hiatt J, Bouhaddou M, et al. Comparative host-coronavirus protein interaction
 380 networks reveal pan-viral disease mechanisms. *Science* (80-). 2020; 370:

381 2. Rohaim MA, El RF, Clayton E, et al. Since January 2020 Elsevier has created a COVID-
 382 19 resource centre with free information in English and Mandarin on the novel coronavirus
 383 COVID- 19 . The COVID-19 resource centre is hosted on Elsevier Connect , the company ' s
 384 public news and information . 2020;

385 3. Millet JK, Whittaker GR. Host cell proteases: Critical determinants of coronavirus tropism
 386 and pathogenesis. *Virus Res.* 2015; 202:120–134

387 4. Hikmet F, Méar L, Edvinsson Å, et al. The protein expression profile of ACE2 in human
 388 tissues. *Mol. Syst. Biol.* 2020; 16:1–16

389 5. Daly JL, Simonetti B, Antón-Plágaro C, et al. Neuropilin-1 is a host factor for SARS-CoV-
 390 2 infection. *bioRxiv* 2020; 865:861–865

- 391 6. Melms JC, Biermann J, Huang H, et al. A molecular single-cell lung atlas of lethal
392 COVID-19. *Nature* 2021;
- 393 7. Reizis B. Plasmacytoid Dendritic Cells: Development, Regulation, and Function.
394 *Immunity* 2019; 50:37–50
- 395 8. Delorey TM, Ziegler CGK, Heimberg G, et al. COVID-19 tissue atlases reveal SARS-
396 CoV-2 pathology and cellular targets. *Nature* 2021;
- 397 9. Voss WN, Hou YJ, Johnson N V., et al. Prevalent, protective, and convergent IgG
398 recognition of SARS-CoV-2 non-RBD spike epitopes in COVID-19 convalescent plasma.
399 *bioRxiv* 2020; 5268:1–11
- 400 10. Garcia-Beltran WF, Lam EC, Astudillo MG, et al. COVID-19-neutralizing antibodies
401 predict disease severity and survival. *Cell* 2021; 184:476-488.e11
- 402 11. Deng X, Garcia-knight MA, Khalid MM, et al. Transmission, infectivity, and
403 neutralization of a spike L452R SARS-CoV-2 variant. *Cell* 2021;
- 404 12. Hoffmann M, Arora P, Groß R, et al. SARS-CoV-2 variants B.1.351 and P.1 escape from
405 neutralizing antibodies. *Cell* 2021; 2384–2393
- 406 13. Chi X, Yan R, Zhang J, et al. A neutralizing human antibody binds to the N-terminal
407 domain of the Spike protein of SARS-CoV-2. *Science* (80-.). 2020; 369:650–655
- 408 14. Zhang L, Jackson C, Mou H, et al. The D614G mutation in the SARS-CoV-2 spike
409 protein reduces S1 shedding and increases infectivity. *bioRxiv Prepr. Serv. Biol.* 2020;
- 410 15. Chaudhari A, Chaudhari M, Mahera S, et al. In-Silico analysis reveals lower transcription
411 efficiency of C241T variant of SARS-CoV-2 with host replication factors MADP1 and
412 HNRNP-1. *bioRxiv* 2020;
- 413 16. Madhavi Sastry G, Adzhigirey M, Day T, et al. Protein and ligand preparation:
414 parameters, protocols, and influence on virtual screening enrichments. *J. Comput. Aided.*
415 *Mol. Des.* 2013; 27:221–234
- 416 17. Shelley JC, Cholleti A, Frye LL, et al. Epik: a software program for pK_a prediction and
417 protonation state generation for drug-like molecules. *J. Comput. Aided. Mol. Des.* 2007;
418 21:681–691
- 419 18. . SC '06: Proceedings of the 2006 ACM/IEEE Conference on Supercomputing. 2006;
- 420 19. van Zundert GCP, Moriarty NW, Sobolev O V, et al. Macromolecular refinement of X-
421 ray and cryoelectron microscopy structures with Phenix/OPLS3e for improved structure and
422 ligand quality. *Structure* 2021;
- 423 20. Steinbrecher T, Abel R, Clark A, et al. Free Energy Perturbation Calculations of the
424 Thermodynamics of Protein Side-Chain Mutations. *J. Mol. Biol.* 2017; 429:923–929
- 425 21. Toukmaji AY, Board JA. Ewald summation techniques in perspective: A survey.
426 *Comput. Phys. Commun.* 1996; 95:73–92
- 427 22. Zielkiewicz J. Structural properties of water: Comparison of the SPC, SPCE, TIP4P, and
428 TIP5P models of water. *J. Chem. Phys.* 2005; 123:
- 429 23. Martyna GJ, Klein ML, Tuckerman M. Nosé-Hoover chains: The canonical ensemble via
430 continuous dynamics. *J. Chem. Phys.* 1992; 97:2635–2643

- 431 24. . pymol.
- 432 25. Kozakov D, Brenke R, Comeau SR, et al. PIPER: an FFT-based protein docking program
433 with pairwise potentials. *Proteins* 2006; 65:392–406
- 434 26. Harlow GR, Halpert JR. Alanine-scanning Mutagenesis of a Putative Substrate
435 Recognition Site in Human Cytochrome P450 3A4: ROLE OF RESIDUES 210 AND 211 IN
436 FLAVONOID ACTIVATION AND SUBSTRATE SPECIFICITY*. *J. Biol. Chem.* 1997;
437 272:5396–5402
- 438 27. Simonsen SM, Sando L, Rosengren KJ, et al. Alanine Scanning Mutagenesis of the
439 Prototypic Cyclotide Reveals a Cluster of Residues Essential for Bioactivity*. *J. Biol. Chem.*
440 2008; 283:9805–9813
- 441 28. Lyne PD, Lamb ML, Saeh JC. Accurate prediction of the relative potencies of members
442 of a series of kinase inhibitors using molecular docking and MM-GBSA scoring. *J. Med.*
443 *Chem.* 2006; 49:4805–4808
- 444 29. Greenidge PA, Kramer C, Mozziconacci JC, et al. MM/GBSA binding energy prediction
445 on the PDBbind data set: Successes, failures, and directions for further improvement. *J.*
446 *Chem. Inf. Model.* 2013; 53:201–209
- 447 30. Beard H, Cholleti A, Pearlman D, et al. Applying Physics-Based Scoring to Calculate
448 Free Energies of Binding for Single Amino Acid Mutations in Protein-Protein Complexes.
449 *PLoS One* 2013; 8:null
- 450 31. Kormos BL, Baranger AM, Beveridge DL. A study of collective atomic fluctuations and
451 cooperativity in the U1A-RNA complex based on molecular dynamics simulations. *J. Struct.*
452 *Biol.* 2007; 157:500–513
- 453 32. Chang S, Hu J, Lin P, et al. Substrate recognition and transport behavior analyses of
454 amino acid antiporter with coarse-grained models. *Mol. Biosyst.* 2010; 6:2430—2438
- 455 33. Fratev F. The SARS-CoV-2 S1 spike protein mutation N501Y alters the protein
456 interactions with both hACE2 and human derived antibody: A Free energy of perturbation
457 study. *bioRxiv* 2020; 2020.12.23.424283
- 458 34. Zhang L, Jackson CB, Mou H, et al. SARS-CoV-2 spike-protein D614G mutation
459 increases virion spike density and infectivity. *Nat. Commun.* 2020; 11:1–9
- 460 35. Jangra S, Ye C, Rathnasinghe R, et al. SARS-CoV-2 spike E484K mutation reduces
461 antibody neutralisation. *The Lancet Microbe* 2021; 1–2
- 462 36. Kufareva I, Abagyan R. Methods of protein structure comparison. *Methods Mol. Biol.*
463 2012; 857:231–257
- 464 37. Bornot A, Etchebest C, de Brevern AG. Predicting protein flexibility through the
465 prediction of local structures. *Proteins* 2011; 79:839–852
- 466 38. Donald JE, Kulp DW, Degrado WF. Define salt bridge. *Biochemistry* 2012; 79:898–915
- 467 39. Meuzelaar H, Vreede J, Woutersen S. Influence of Glu/Arg, Asp/Arg, and Glu/Lys Salt
468 Bridges on α -Helical Stability and Folding Kinetics. *Biophys. J.* 2016; 110:2328–2341
- 469 40. Lee JI, Pung Pung Hwang, Wilson TH. Lysine 319 interacts with both glutamic acid 269
470 and aspartic acid 240 in the lactose carrier of *Escherichia coli*. *J. Biol. Chem.* 1993;
471 268:20007–20015

